Combined Electromagnetic and Piezoelectric Shaker System for High Frequency Environment Testing

Jacob Cox[1], McKaelin Edralin[1], Matthew S. Allen[*2], Michael Denison[3], Troy J. Skousen[3] and Washington De Lima[4]

[1]Undergraduate Students, Brigham Young University, Department of Mechanical Engineering
[2]Professor, Brigham Young University, Department of Mechanical Engineering, matt.allen@byu.edu
[3]Technical Staff, Sandia National Laboratories[*]
[4]Honeywell Federal Manufacturing and Technologies,[†] wdelima@kcnsc.doe.gov

Abstract

A prior work [Singh, Allen et al., Experimental Techniques, 2022] showed that piezoelectric actuators could be combined with electrodynamic shakers to impart wideband random vibration input to a Device Under Test (DUT) up to 5kHz, while significantly reducing the drive voltages required for an electrodynamic shaker alone. The goal of such a system is to use electrodynamic shakers and piezoelectric actuators together for low and high frequencies respectively, where each is most effective. At the same time, the piezoelectric actuators provide additional inputs that may overcome the anti-resonances at the electrodynamic shaker head, where the nodes of a major mode reside in the single input system. This work builds on that effort, presenting the design and characterization of a general system that incorporates several piezoelectric actuators in series with a large electrodynamic shaker to impart a wider broadband input to a DUT. A model is presented which was used to facilitate the design. The model was calibrated by comparing measured and predicted transfer functions between the DUT accelerations and the actuator input voltages. Particular attention is given to the model for the piezoelectric actuator and amplifier. This is shown to be a limiting factor which depends on the number of actuators available and the current that the amplifiers can supply. Measurements are presented from the completed system with quantified capabilities.

Keywords: Electrodynamic Shaker, Piezoelectric Actuator, Random Vibration Environment

1 Introduction

Mechanisms and electronics in rockets, aircraft, and automobiles are often subject to a high-vibration environment. To ensure the reliability and durability of these components, they are tested using electrodynamic shakers, which use an electromagnetic force to generate controlled vibrations. While current electrodynamic shakers are capable of producing large forces, they do have failure limits. One such limit is associated with high frequency resonances as studied in [1], that lead to mechanical failure of the shaker armature which in turn limits their frequency range to below about 2000 Hz. Attempting to exceed this frequency range can cause catastrophic failure, as shown in Figure 1, requiring expensive and project-delaying repair or maintenance. This limitation poses an issue because many mechanical and electrical components experience significant vibration environments up to 5000 Hz.

Romero et al. [2] seem to have been the first to combine piezoelectric actuators such as these with other systems to reproduce combined environments. This work builds on a recent study by Singh et al. [3], who demonstrated that piezoelectric actuators could be integrated with an electrodynamic shaker to enable testing from 2000 - 5000 Hz. In that work, the electrodynamic shaker was operated between 100-2000 Hz, with the piezoelectric actuators providing the forces needed from 2-5kHz, thus creating a high-frequency environment. Despite Singh's promising results, much remains to be understood regarding the best

Figure 1: Catastrophic failure due to an electrodynamic shaker being driven at a resonance in which the armature bends, leading to excessive stresses in the cylindrical part that is shown.

practices in designing and modeling practical piezo actuator configurations. Furthermore, we desired to create a system that was modular, with a plate where test articles could be mounted just as they are in conventional shaker systems.

During the 2023-2024 academic year, Sandia National Laboratories enlisted a team of undergraduate Mechanical Engineering students to create a modular system that combined a large shaker with a set of PPA40XL piezoelectric actuators, to enable regular environmental tests at high frequencies, using the approach envisioned by Singh et al. [3]. The system consisted of a base plate that interfaced with a 2000-lbf LDS V830–335 Shaker at BYU, but with a bolt pattern that would also be compatible with Unholtz-Dickie shakers at Sandia Labs. The system was to consist of a top plate with a standard bolt pattern, where a variety of test articles could be attached. The team completed the design, as detailed in this report, yet did not have time to resolve all of the issues with the modeling and testing of the system. Authors Cox and Allen subsequently completed testing and resolved issues with the modeling, and their findings are summarized here, as well as the design that was created and the analysis and considerations that led to the design.

Hence, this paper builds on the work of Singh et al. [3] by presenting the design of the piezo/electromagnetic shaker system that the students developed and presenting models that capture its axial dynamic behavior. Measurements from the completed system are provided, highlighting its capabilities, the accuracy of our models, and offering suggestions for future iterations on the MIMO test system.

2 Methods

2.1 System Design

The final design is shown in Figure 2. The five major components are more thoroughly detailed in Figures 2-4 and the descriptions that follow.

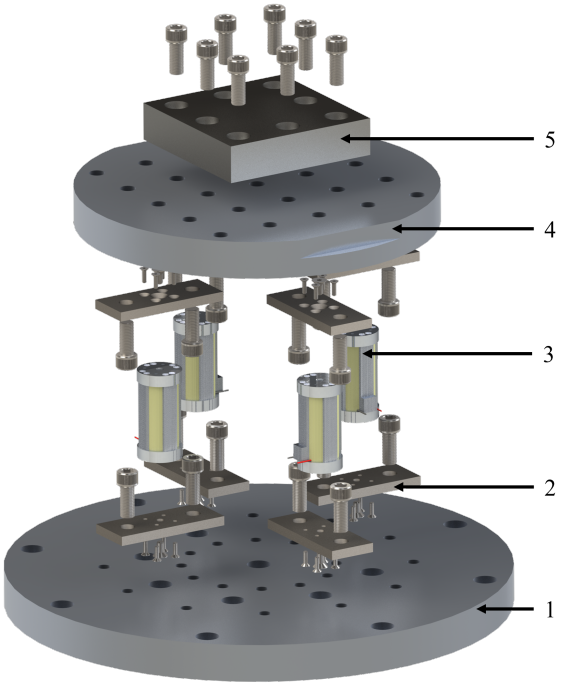

Figure 2: Exploded CAD view of the piezo assembly with the following components: 1) base plate (designed to be mounted to the top of a large shaker), 2) mounting brackets, 3) PPA40XL piezoelectric actuator, 4) top plate, and 5) mass that simulates the loading of a DUT.

1. The base plate serves as the foundation of the system, connecting the electrodynamic shaker and piezoelectric actuators. The dimensions and hole layout can be seen in Figure 3. The plate features two hole patterns: one for connecting it to the electrodynamic shaker and the other for attaching the piezo actuator mounting brackets, as shown in Figures 2 and 4.

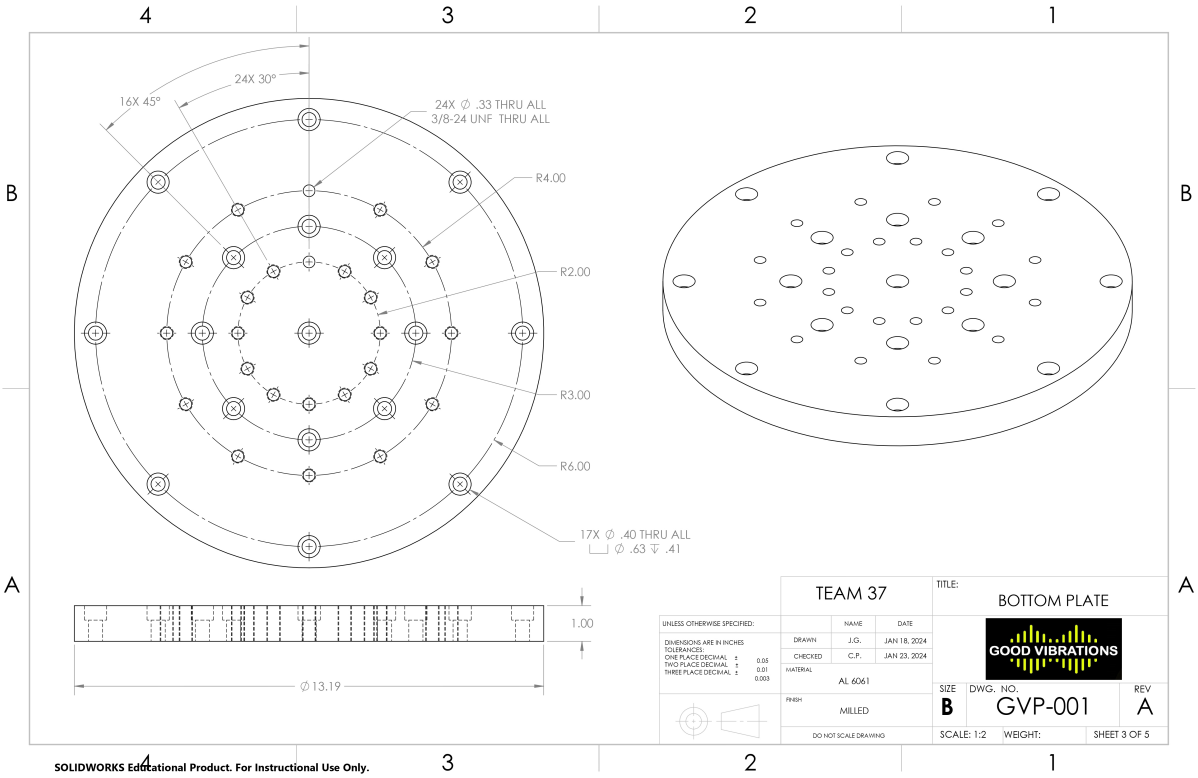

Figure 3: Bottom plate part drawing. This design allows for a 2, 4, 6, and 8 piezo actuator configuration.

2. The mounting brackets secure the piezo actuators to the top and bottom plates and ensure they are level to prevent overstraining. According to the manufacturer, the piezo actuators are machined with a height tolerance of 200 μm. However, their maximum tensile strain is 15.5 μm. Hence, there was concern that they could exceed this strain when

bolted into the assembly. To address this, the bracket design shown in Figure 4 allows shim stock to be used between each bracket and the top and bottom plate, so one can avoid over-straining when assembling the system. The mounting brackets were also precisely machined and sanded to within 2.5μm. (It should be noted that this design only works for a maximum of four piezo actuators because the edges would interfere if more piezo actuators were used. A modified mounting bracket was also designed that allows for more piezo actuators but was not used in this study. This modified design can be seen in Figure 24 in the Appendix.)

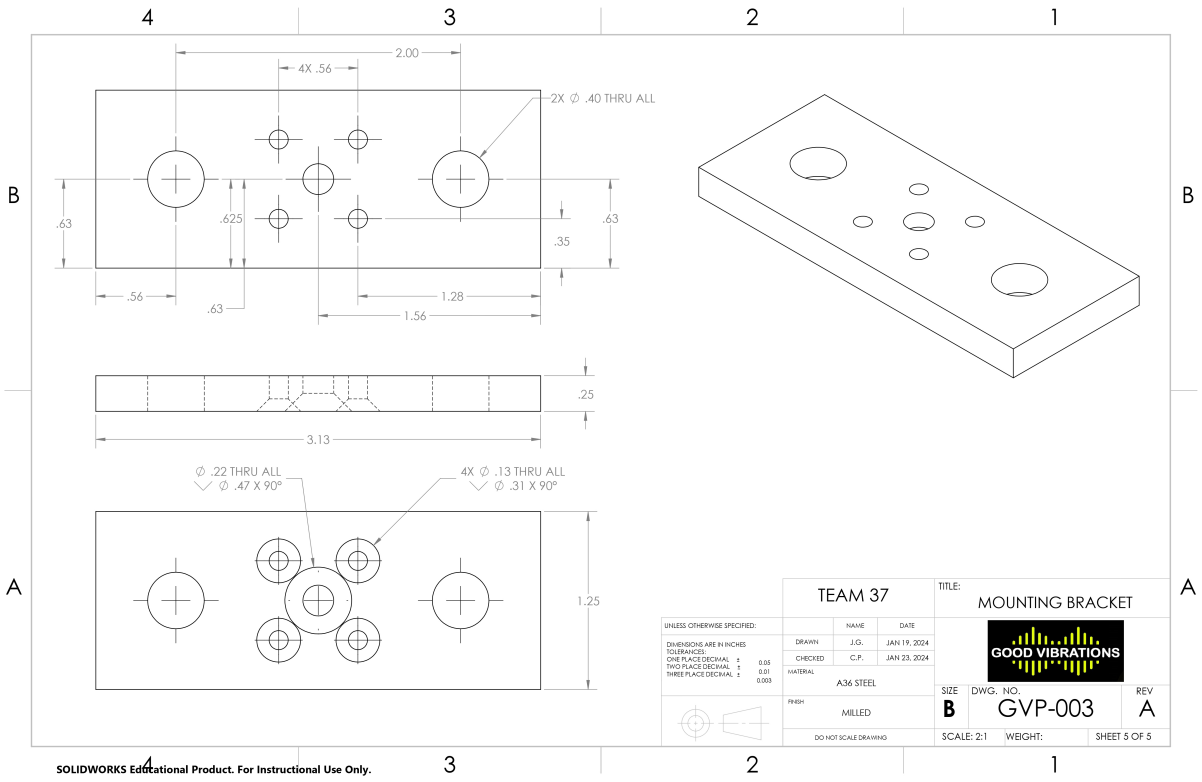

Figure 4: Mounting bracket design used for four or fewer piezo actuators

3. The piezoelectric actuators utilized in this research were PPA40XL parallel pre-stressed actuators from Cedrat. Piezoelectric actuators convert an electrical signal into a displacement through the use of quartz crystals. In this system, the piezoelectric actuators exert a force between the EM shaker and the top plate to supplement that provided by the EM shaker.

4. The top plate interfaces with the mounting brackets and transfers forces to the DUT. A finite element model (FEM) was used to predict the modes of the plate in free-free conditions and are shown in Fig. 6. Most of the modes have nodes at the plate center, so they won't affect the displacement of a DUT mounted there. Hence, the focus was on maximizing the frequency of Mode 3 so as to minimize its influence on the DUT motion. Furthermore, when the piezos and top plate are mounted to the shaker, there is a mode in which the top plate bounces on the piezos. This reveals that a tradeoff exists. The plate should be small and thick to maximize the frequency of the flexible mode, and yet it should be as light as possible (and hence as thin as possible) to maximize the bounce mode frequency. Ultimately, a 9.5 × 1-inch plate was chosen to balance these competing objectives. However, as will be seen later, the final results suggest that more should have been done to minimize the mass of the top plate.

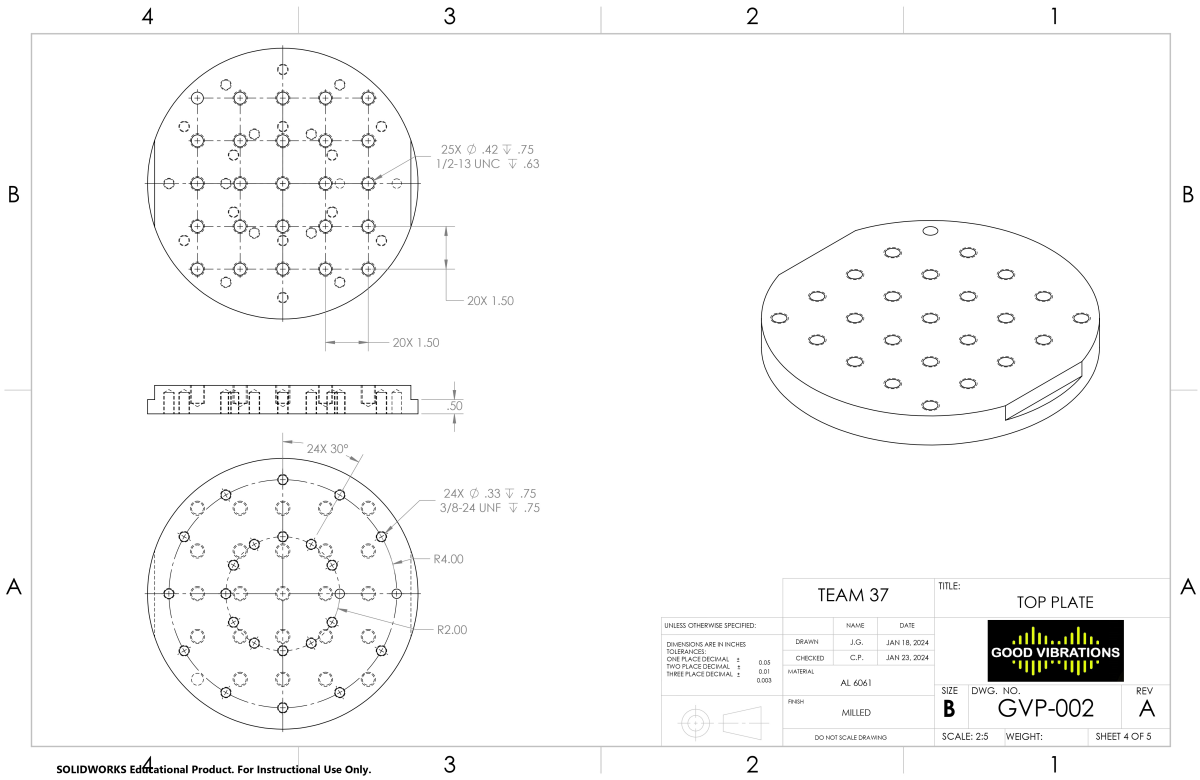

Figure 5: Top plate part drawing

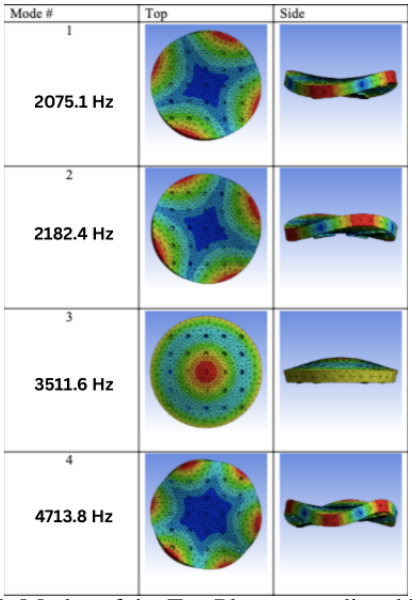

Figure 6: Modes of the Top Plate as predicted by FEM

5. The DUT is the mechanical or electrical device subjected to testing. For this research, the DUT is a rigid block of aluminum that has similar mass and stiffness to a typical DUT. Unfortunately, time constraints did not allow the system to be tested with the DUT attached, so all results presented in this paper are for the system with a bare top plate.

Many components of the piezo assembly are costly. To ensure that the piezo assembly would not break, could survive repeated use, and would meet desired performance metrics, a discrete mass model was created that predicts the dynamic behavior of the system in the axial direction. Using this model, two major failure criteria were analyzed, the voltage and strain limits of the piezo actuators. Later, the current limit of our amplifier was found to be a limiting factor and was added to this analysis.

Once the system was assembled these models were evaluated against experimental measurements. The models were then tuned using experimental data. Using these updated models, we hope to more confidently predict the behavior of other design variations. Therefore, in the following sections, results are presented for both the initial and updated models.

2.2 Discrete Mass Model: MATLAB

A discrete spring-mass model of the system was created to size the actuators and obtain preliminary performance estimates. Simulations of this model were implemented in a MATLAB script. The system was modeled as a 3DOF system, shown in Figure 7. Two masses represent the EM shaker and capture its first axial mode, while the other mass represents the top plate and DUT, both of which sit on top of the piezo actuators.

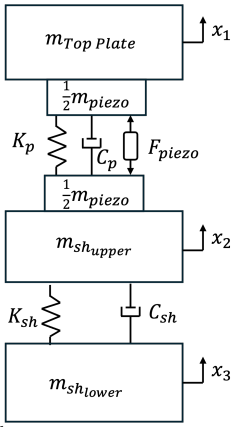

Figure 7: 3DOF model of the shaker assembly. The top mass represents the top plate, with K_p the total equivalent spring constant of all four piezo actuators, C_p the total equivalent damping coefficient, and m_{piezo} the mass of four piezos and required brackets. The shaker is modeled as a two DOF system, with the armature mass split between the upper mounting surface $m_{\text{sh,u}}$ and the lower portion $m_{\text{sh,l}}$. K_{sh} is the shaker stiffness and C_{sh} is the damping coefficient of the shaker.

Using this model, a mathematical model of the system was developed as follows:

$$\mathbf{M}\ddot{\mathbf{x}} + \mathbf{C}\dot{\mathbf{x}} + \mathbf{K}\mathbf{x} = \mathbf{F} \tag{1}$$

where $\mathbf{x} = [x_1, x_2, x_3]^{\mathrm{T}}$ are the displacements of the masses shown in Figure 7.

$$\mathbf{M} = \begin{bmatrix} m_{\text{Top Plate}} + \frac{1}{2}m_{\text{piezo}} + m_{\text{payload}} & 0 & 0 \\ 0 & m_{\text{sh,u}} + \frac{1}{2}m_{\text{piezo}} & 0 \\ 0 & 0 & m_{\text{sh,l}} \end{bmatrix}, \quad \mathbf{C} = \begin{bmatrix} C_p & -C_p & 0 \\ -C_p & C_p + C_{\text{sh}} & -C_{\text{sh}} \\ 0 & -C_{\text{sh}} & C_{\text{sh}} \end{bmatrix}, \tag{2}$$

$$\mathbf{K} = \begin{bmatrix} K_p & -K_p & 0 \\ -K_p & K_p + K_{\text{sh}} & -K_{\text{sh}} \\ 0 & -K_{\text{sh}} & K_{\text{sh}} \end{bmatrix}, \quad \mathbf{F} = \begin{Bmatrix} F_{\text{piezo}} \\ -F_{\text{piezo}} \\ F_{\text{sh}} \end{Bmatrix}, \tag{3}$$

It is worth noting a deviation from the model presented by Singh et al. [3]. In their model, the shaker force was applied to the upper shaker mass. In contrast, our model applies the shaker force to the lower mass. This aligns with the functionality of our electrodynamic shaker, where the applied force is generated by coils at the bottom of the armature. This approach was also found to better match the experimental behavior of our system, which is presented later.

The values of all of the constants used are listed in Table 1. Initially, values from Singh et al. [3] were used, supplemented by measured mass characteristics of the new system. However, damping and stiffness values were later tuned, matching the theoretical transfer functions to the experimental ones (see Sections 2.6 and 3.2 for additional information on experimental transfer function collection and tuning results).

Once the mechanical system was defined, transfer functions relating the shaker and piezo input forces to the displacement of each mass were found as follows. Starting with Eq. (1), the force vector can be separated into components, resulting in Eq. (4).

$$\left[-\omega^2\mathbf{M} + i\omega\mathbf{C} + \mathbf{K}\right]\mathbf{X}(\omega) = F_{\text{sh}}(\omega)\begin{bmatrix}0\\0\\1\end{bmatrix} + F_{\text{piezo}}(\omega)\begin{bmatrix}1\\-1\\0\end{bmatrix} \tag{4}$$

Treating each force individually, the transfer functions become Eqs. (5) and (6), where the rows of $\mathbf{H}_{x,F_i}$ refer to the transfer functions from the input force to the displacement of: 1.) the top plate, 2.) the top of the EM shaker, and 3.) the bottom of the EM shaker, respectively.

Table 1: The parameters used in the 3DOF MATLAB model.

Parameter	Definition	Initial Method	Initial Value	Final Method	Final Value
m_{piezo}	Mass of piezo (kg)	Direct Meas.	0.195	Direct Meas.	0.195
m_b	Mass of Brackets (kg)	Direct Meas.	0.17	Direct Meas.	0.17
m_{sh}	Total mass of shaker armature (kg)	Shaker Spec.	12.83	Shaker Spec.	12.83
$m_{\text{sh,u}}$	Upper mass of shaker armature (kg)	Exper. Calib.	10.89	Exper. Calib.	10.89
$m_{\text{sh,l}}$	Lower mass of shaker armature (kg)	Exper. Calib.	1.94	Exper. Calib.	1.94
m_{TP}	mass of top plate (kg)	Direct Meas.	2.905	Direct Meas.	2.905
K_p	Piezo stiffness (N/m)	CEDRAT catalog	1.59e8	Exper. Calib.	3.66e7
C_p	Damping within the piezo (N*s/m)	CEDRAT catalog	90.74	Exper. Calib.	544.44
K_{sh}	Shaker armature stiffness (N/m)	Exper. Calib.	3e8	Exper. Calib.	2.97e8
C_{sh}	Damping within the shaker (N*s/m)	Modal Analysis	7.82e3	Exper. Calib.	1.56e2
m_{payload}	Mass of payload being driven (kg)	-	0	-	0
F_f	Force Factor (N/V)	CEDRAT catalog	186.7	Exper. Calib.	46.7

$$\mathbf{H}_{x,F_{\text{sh}}}(\omega) = \left[-\omega^2\mathbf{M} + i\omega\mathbf{C} + \mathbf{K}\right]^{-1} \begin{bmatrix} 0 \\ 0 \\ 1 \end{bmatrix} \tag{5}$$

$$\mathbf{H}_{x,F_{\text{piezo}}}(\omega) = \left[-\omega^2\mathbf{M} + i\omega\mathbf{C} + \mathbf{K}\right]^{-1} \begin{bmatrix} 1 \\ -1 \\ 0 \end{bmatrix} \tag{6}$$

The required forcing signal was then calculated using Eq. (7), where $a(\omega)$ represents the desired acceleration environment, and the transfer function H_{1,F_i} in the denominator is multiplied by $-\omega^2$ to convert the displacement transfer functions in Eqs. (5) and (6) from displacement to acceleration over force.

$$F_i(\omega) = \frac{a(\omega)}{-\omega^2 H_{1,F_i}(\omega)}, \text{ where } i = (\text{sh, piezo}) \tag{7}$$

This was done for both the shaker and piezo input forces as if they were individually responsible for recreating the entire environment. Afterwards, the forcing signals were set to zero over certain frequency ranges so that the shaker was fully responsible for recreating the environment up to a cut-off frequency (typically 1700 Hz) and the Piezos provided the environment from the cut-on frequency (typically 500 to 1700 Hz) up to the maximum frequency (typically 5000 Hz). Then the forcing signals were multiplied by the displacement transfer functions to simulate the movements of each of the masses.

$$\mathbf{X}(\omega) = \mathbf{H}_{x,F_i}(\omega) F_i(\omega) \tag{8}$$

2.3 Piezo Voltage Limits

In addition to the mechanical system, the electronics also needed to be characterized in order to correctly size the actuators and predict failure. As in Singh [3], a linear force to voltage relationship was assumed and characterized by a force factor (F_f), as given in Eq. (9). Combining this relation with our forcing functions, the time domain voltage signal for any acceleration environment could be calculated and compared to the voltage limits of the piezo actuators.

$$V_{piezo} = F_{piezo}\frac{V_{max}}{F_{max}} = \frac{F_{piezo}}{F_f} \tag{9}$$

The allowable voltage range for the piezo actuators is -20 to 150V. They are driven through an amplifier that increases the voltage by a factor of 20 with a DC bias so that the input to the amplifier can be centered at zero. With a DC bias of 65V, the maximum sinusoidal signal is 85V (or 85/20 = 4.25V at the output of the control software). To account for the DC bias and amplifier inaccuracies, the amplitude was limited to 75V in this study, which provided a 10V buffer.

2.4 Piezo Strain Limits

The manufacturer specifies the maximum tensile strain for the actuator to be 15.5 μm. The maximum compressive strain is not given, but the maximum resonant displacement is specified to be 27 μm peak-to-peak, so that the maximum vibration amplitude is approximately the same as the maximum tensile strain. They also state the maximum strain of the piezoelectric material is 0.12%, which would correspond to a total displacement of about 48 μm. The largest displacement that the piezo actuators can create is nominally 43 μm [**?**]. In operation, the displacement consists of the dynamic movement of the system during testing and a static displacement caused by the 65V DC bias. Hence, it seems that the system can survive 21.5 μm of displacement about the biased state.

In this work, the dynamic portion of the displacement was estimated by transferring the displacements obtained from Eq. (8) into the time domain and then taking the difference $(x_2 - x_1)$ to find the stretch in the piezos. The static portion (D_s) is calculated using the force factor and stiffness of the piezos as follows:

$$D_s = \frac{V_{bias} F_f}{K_p} \tag{10}$$

While some of this stretch may actually be taking place in the bolted bracket assembly, it is conservatively assumed that the stretch takes place entirely inside of the piezos.

2.5 Amplifier Current Limits

The electrical current capabilities of the amplifier provide another limitation. In this research, two amplifiers were utilized, each capable of outputting 6.8A, which was found to limit the maximum frequency and displacement amplitude the actuators could achieve. The piezo actuator expansion is dependent on the speed with which the amplifier can fill the capacitance of the quartz. At 0V and room temperature, the capacitance of an individual actuator is reported as c = 17 μF. For our modeling, the capacitance was multiplied by a factor to account for temperature and voltage effects per the recommendations found here [4]. These effects seem consistent with those mentioned in Sherrit et al. [5], yet the authors were not able to find any literature that reported actual data as was available on [4]. In this work, a factor of 1.4 was selected, based roughly on our maximum voltage amplitude and operation at room temperature.

Using the fundamental equation for current through a capacitor,

$$I = c\frac{dV}{dt} \tag{11}$$

The frequency domain current signal can then be calculated from the voltage signal and then converted to the time domain using an inverse Fourier transform. The amplifier current was found to be the strongest limiting factor for shaker performance. Consequently, two analyses were performed to better understand the effects of exceeding our current limits. First, the amplifier limits were quantified by considering sinusoidal inputs at various frequencies. While each piezo actuator could be driven by a separate amplifier, in this work, only two amplifiers were available and so each amplifier drove two piezo actuators. Given the limits on I (two amplifiers) and c (four piezos with 17 μF each and a temperature factor of 1.4), the maximum value of the derivative $\frac{dv}{dt}$ = 13.6 A / 95.2 μF = 142857 $\frac{V}{s}$. The value of $\frac{dv}{dt}$ that is needed depends on frequency. If we desired to supply a sinusoidal voltage to the piezo actuators at a voltage amplitude of V_p, i.e.

$$V(t) = V_p \sin(\omega t) \tag{12}$$

then the derivative would be

$$\frac{dV}{dt} = V_p \omega \cos(\omega t) \tag{13}$$

and its maximum value is $V_p\omega$. Hence, when $V_p = 75$ V the highest frequency at which the amplifier can achieve the required $\frac{dV}{dt}$ is 303.2 Hz. Conversely, the voltage amplitude V_p would have to be limited to reach the desired peak frequency of 5 kHz. The largest input voltage at 5 kHz is thus found to be 4.55 V.

To verify these calculations, tests were performed in which a sinusoidal input was supplied to the amplifier with two piezo actuators connected to each channel and the voltage out of the amplifier was recorded and is shown in Figure 8. When a low voltage was used, for example, the curves labeled 50 mV (the entries in the legend are the voltage amplitude sent to the amplifier), the output is 0.91 V (1 V expected) whether the frequency is 2 kHz or 5 kHz. As the input voltage increases to 200

or 250 mV the output from the amplifier scales nearly as expected to 3.42 V (4 V expected) and 4 V (5 V expected) when the frequency is 2 kHz. Both of these are within the 11.37 V limit computed using the equations above. Specifically,

$$\frac{dV}{dt} = 142857\frac{\text{V}}{\text{s}} = 11.37\frac{\text{V}}{\text{Channel}} \times (2000 \times 2\pi)\,\frac{\text{rad}}{\text{s}} \tag{14}$$

In contrast, when the frequency is increased to 5 kHz, the output from the amplifier distorts noticeably and the voltage amplitude is only 3.18 V when 5 V were expected. The peak voltage computed for the amplifier for this case, using Eq. (13) is 4.55 V, which is about 40% higher than the voltage that seems to have been achieved. These tests provide evidence that our amplifier current limits likely inhibit the performance of our system, and that the model in the equations above gives a reasonable approximation of the system's behavior.

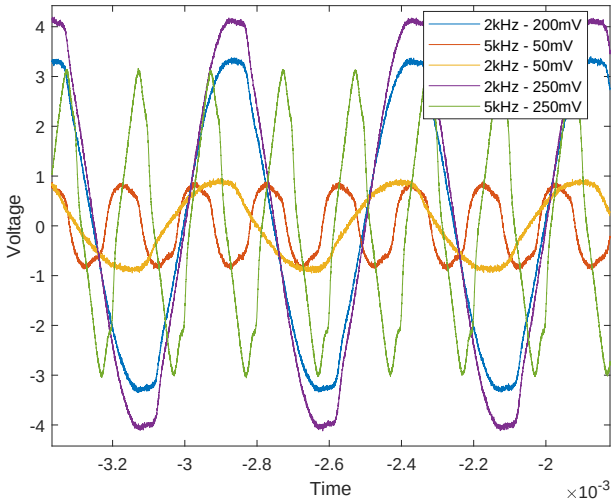

Figure 8: Voltages from piezo amplifier for various input levels

The current limits were also evaluated using our discrete mass model. When simulating the performance of the system, the required current signal calculated from Eq. (11) was crudely clipped, more specifically, all current values exceeding our limits were set to the limit (in the time domain). Then, this updated current was run through the relations presented previously to find the resultant acceleration environment (i.e. Eq. (11), (9), and (7) in that order). The results are presented in Sec. 3.

2.6 Experimental Test Procedure

After the initial round of modeling, the system was designed, manufactured and tested. All tests were performed without a DUT attached, as shown in Fig. 9. Experimental transfer functions were measured between the input voltages to the shaker and piezos and the different accelerometers using DataPhysics SignalCalc software. These are compared with those from the model in the following sections.

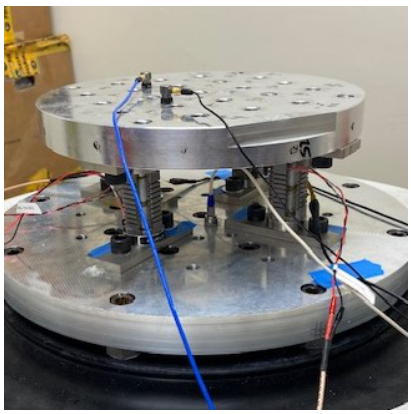

(a) Isometric view of original accelerometer placement

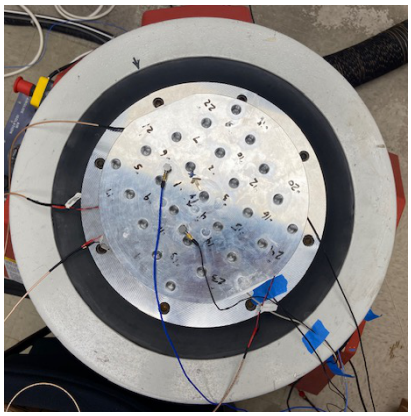

(b) Top-Down view of original accelerometer placement

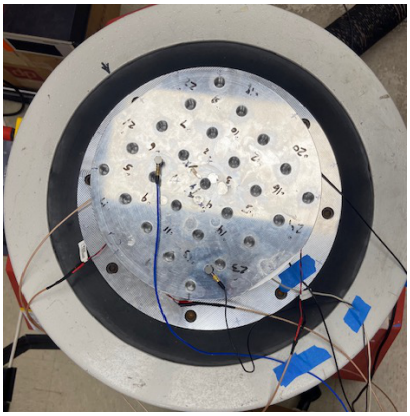

(c) Top-Down view of adjusted accelerometer placement

Figure 9: Accelerometer placement during environment testing

Environment Testing was performed using SignalStar Matrix vibration controller software. For these tests, the software was set to utilize two output signals, one for the electromagnetic shaker and one for the piezos. A single output channel was split to the two piezo amplifiers, each of which fed two of the four piezos. That signal first passed through a high pass filter (Krohn-Hite Variable Filter 3341) with a cutoff frequency of f_{HP} =500 to 1400 Hz, depending on the test. The control signal for the big shaker was fed through a low pass filter (same model) with a cutoff frequency of f_{LP} =1800 Hz. Originally, one of the two accelerometers on the top plate, placed as shown in Figure 9a and 9b, was used as the control. However, further testing revealed that moving one accelerometer outward, to the position shown in Figure 9c, allowed the controller to recreate somewhat more powerful environments.

3 Results

3.1 Model Verification: Modal Test

To better understand the potential limitations of the lab setup, a roving hammer test was performed on the whole piezo assembly while attached to the shaker as shown in Figure 9a. Three accelerometers were included in the test, two on the top plate and one in the center of the base plate, and twenty force locations were used: 8 on the base plate and 12 on the top plate. The approximate accelerometer and forcing locations are labeled in Figure 10. The accelerometers were uniaxial, pointed in the direction of the shaker's force, and remained at the same locations in the qualification tests as shown in 9b, and were judged to be sufficient to observe all modes. The forcing locations were selected to allow the mode shapes of the system to be adequately visualized.

The composite FRF measured in the modal test is shown in Figure 11. There are seven clearly identifiable modes in the FRF. The natural frequencies and damping ratios, along with the descriptions of these mode shapes are given in Table 2. The operating deflection shape at 1427 Hz is also included in Figure 12, since this frequency is of interest later.

The key modes of interest are the bounce mode of the top plate on the piezos and the axial mode of the shaker. Mode 3 at 1179.5 Hz is likely the bounce mode, although the identified mode shape shows that it also involves some rotation of the top plate and perhaps slight deformation or bubbling. This suggests that the DUT might not move uniformly in the vertical direction even if it is mounted at the center of the top plate. (The system also has two lateral modes at lower frequencies of 815.6 and 991.1 Hz.) The axial mode of the shaker can be discerned to reside between 2022.5 and 2180.9. The top plate should have two asymmetric bending modes in this frequency range, yet the measurements show three, so the shaker's axial mode is likely coupled with these, causing an additional resonance that manifests with a similar shape.

The first bubble mode of the top plate is found to occur at 3057.7, which is similar to the 3511.6 Hz frequency predicted by the free-free FEM in Fig. 6, presumably lowered due to the mass added by the piezos.

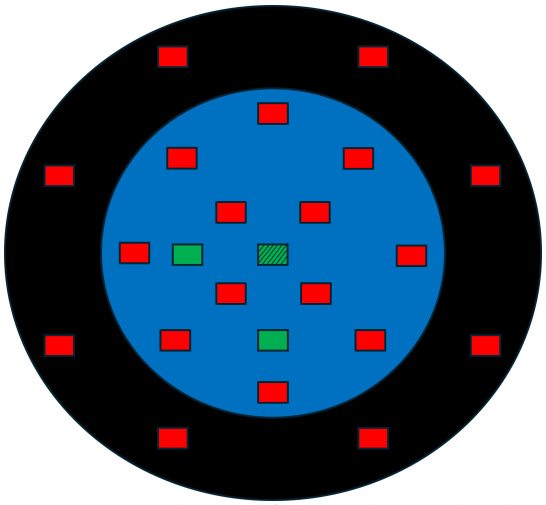

Figure 10: Approximate accelerometer (green rectangles) and force (red rectangles) locations on the top plate (blue) and base plate (black). Note that the center accelerometer was actually on the base plate.

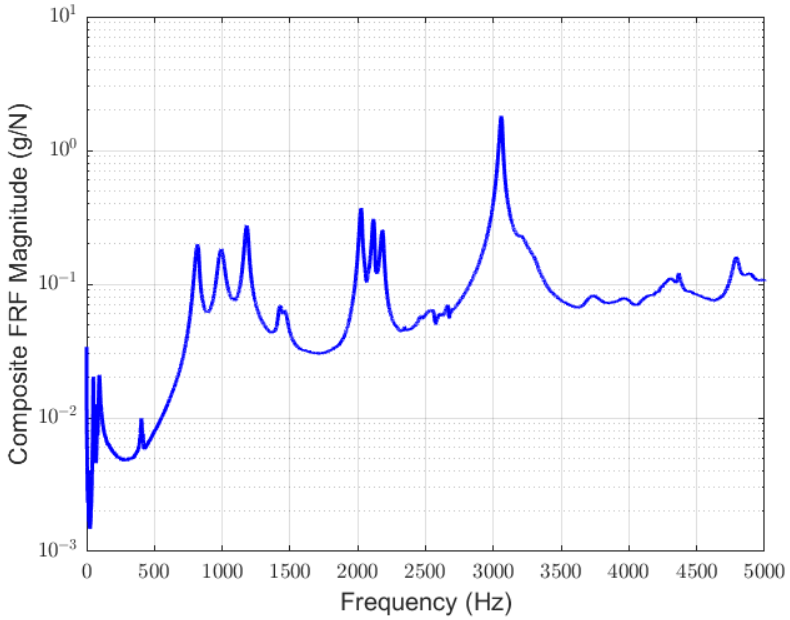

Figure 11: Composite FRF Measured in Modal Test

Table 2: Natural frequencies, damping ratios, and descriptions of measured mode shapes

Mode Number	Natural Frequency (Hz)	Damping Ratio (%)	Top Plate Motion	Base Plate Motion
1	815.6	1.8	Rocking	Vertical Translation
2	991.1	2.2	Rocking	Slight Rocking
3	1179.5	1.2	Rocking and Bubble	Vertical Translation
4	2022.5	0.5	Asymm. Bending	Slight Asymm. Bending
5	2115.7	0.4	Asymm. Bending	Slight Translation
6	2180.9	0.5	Asymm. Bending	Base Plate Twist
7	3057.7	0.4	Bubble	Vertical Translation

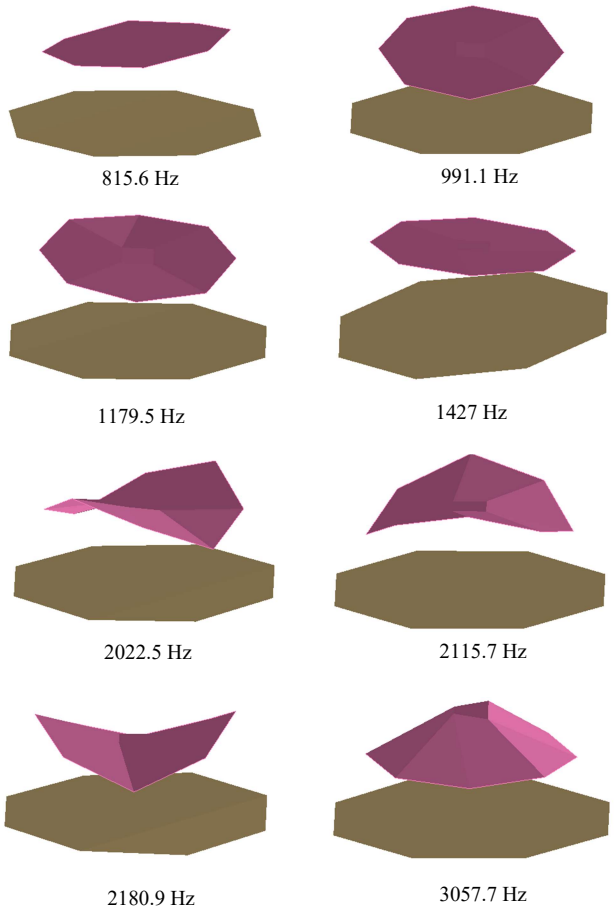

Figure 12: Operating deflection shapes near natural frequencies as measured in the modal test

3.2 Discrete Mass Model

The 3DOF discrete mass model of the shaker has two elastic modes. One would expect the first mode to be one in which the top plate bounces on the shaker, and the second to be the axial mode of the shaker. However, the actual modes generally involved motion of all three masses. In any event, using the original model parameters, the elastic modes occurred at 1989.6 and 2448.2 Hz, considerably higher than the values found in the modal test. The model was tuned in order to better capture the frequency responses presented below, and after this tuning the elastic modes occurred at 1087.8 and 2136.7 Hz.

The discrete mass model was used to reproduce the FRFs of the system, and also to simulate environmental tests, as presented in the figures below. For clarity, results from the initial model are always shown in blue while the updated model is shown in black.

In Figs. 13a-b, the resulting transfer functions from our discrete mass model are compared with the experimental results. The initial model only shows one peak in the FRF (at about 2500 Hz); the lower frequency mode apparently does not respond. The updated model captures both of the experimentally observed resonances. Except for the transfer function from the shaker to the bottom of the piezos, the initial model tends to follow the same general trend of the experimental data. Although the updated model significantly improves in capturing the true behavior of the system at frequencies below 2500 Hz. As shown in Table 1, the model updating primarily consisted in reducing the piezo stiffness and damping from the values in the catalog and reducing the shaker damping relative to the value that was initially assumed. The model does not include any of the asymmetric modes nor any modes beyond 2500 Hz, so it is not expected to match the measurements above that frequency.

Recall that the control scheme used in these simulations only employs the electromagnetic shaker below 1700 Hz and then only the piezos above that frequency. Hence, the predictions of strain, voltage, and current presented in the following only use a portion of each of the transfer functions shown in Figs. 13. Therefore, the significant discrepancy between the shaker's

experimental and updated model at high frequencies, for example, does not affect the accuracy of our results.

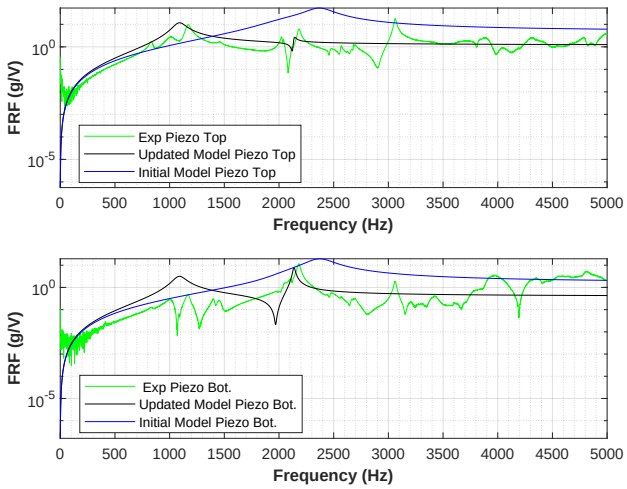

(a) $H_{1,F_{\text{piezo}}}$ and $H_{2,F_{\text{piezo}}}$ (piezo as input)

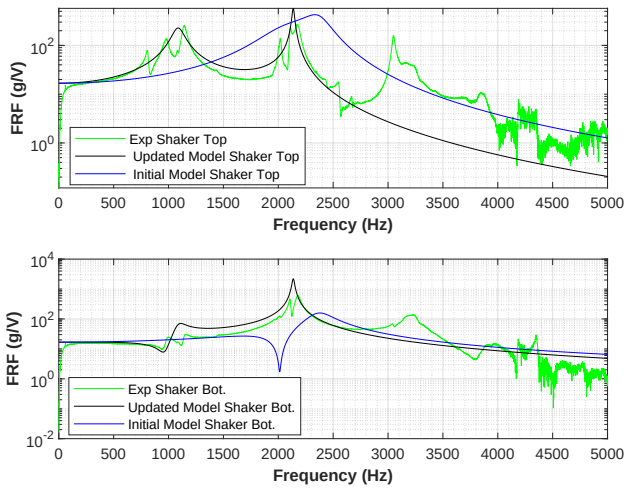

(b) $H_{1,F_{\text{sh}}}$ and $H_{2,F_{\text{sh}}}$ (shaker as input)

Figure 13: Experimental and theoretical transfer functions from the force inputs to the accelerations at the top and bottom of the piezos. Since the voltage-to-force relationship of the shaker is unknown, the models for Figs. 13b show the transfer functions after multiplying by a factor to match the general magnitude of the experimental data. The experimental data for the Piezo top is an average of the transfer functions of both accelerometers.

The rest of the results presented in this section concern the case in which piezo and shaker forces were determined to replicate a target environment of 0.1 g^2/Hz at the DUT from 10 to 5000 Hz. The required forces were computed using Eq. (7). We approximate the system as behaving as a perfect high/low pass filter at 1700 Hz, so the electromagnetic shaker forces were set to zero from 1700.25 to 5000 Hz and the piezoelectric actuator forces were set to zero from 0 to 1700 Hz. These forces were applied to the models in Eqs. (5) and (6) to find the displacements and hence the accelerations of each mass, and those responses were added to find the response of the DUT and of the rest of the system. The resulting environment had a root mean square amplitude of 22.4 g.

Figure 14 displays the predicted stretching in the piezo actuators as a function of time. Notably, the maximum stretch does not exceed the stated limits (43 μm) for these actuators. Initially, the magnitude of stretching may seem surprising, considering the overall amplitude of the vibration environment and the low frequencies involved. Further analysis shows that the shaker input at low frequencies does cause larger displacements. However, the top plate and upper shaker mass move in tandem, causing little to no stretching in the actuators as seen in the time domain in Figure 15.

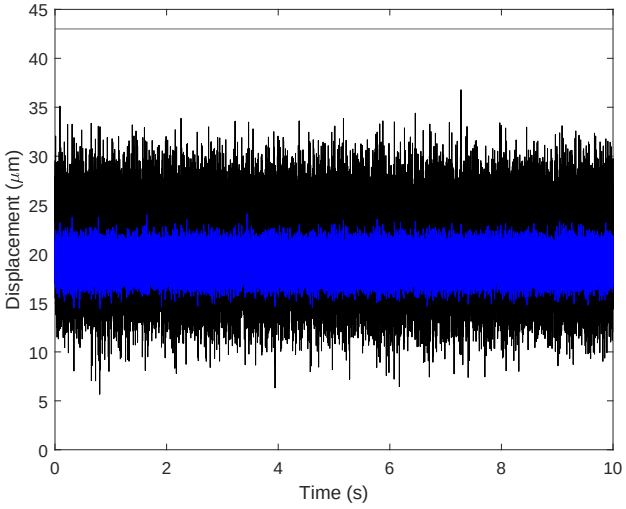

Figure 14: Stretch in the piezo actuators versus time for the (blue) initial model and (black) updated model.

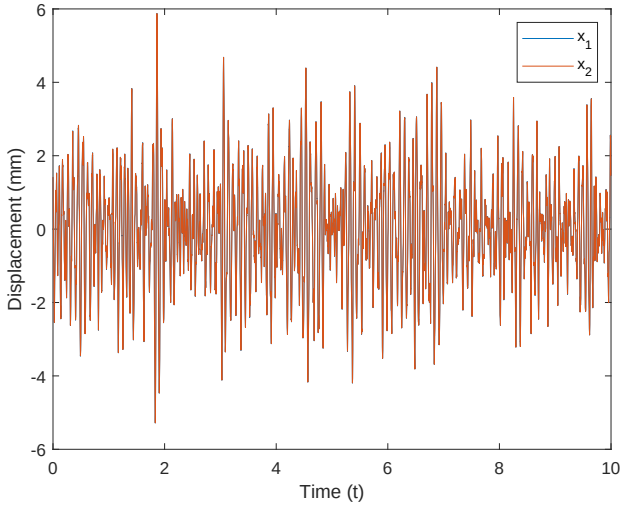

Figure 15: Displacements of the top and middle masses over time taken from the simulation of the updated model.

Similarly, the voltage capacities of the piezos were not found to be a limiting factor for this level of environment. The time histories were created by taking the inverse Fourier transform of the piezo driver signal (see Eq. (9), which is zero from 10-1700Hz. Figure 16 shows the voltage signals from our initial and updated models. Interestingly, the two plots show a strong difference. While the initial model predicts a max voltage of 8.6 V, the updated model predicts a max voltage of 60.6 V, more than a 7-times difference. This isn't surprising considering the fact that the transfer function of the initial model was an order of magnitude larger at high frequencies, as shown in Figure 13a. One large contributing factor is that when tuning the model, the force factor (F_f) for the piezos was reduced by a factor of 4 in order to match the overall magnitude of the experimentally measured transfer functions.

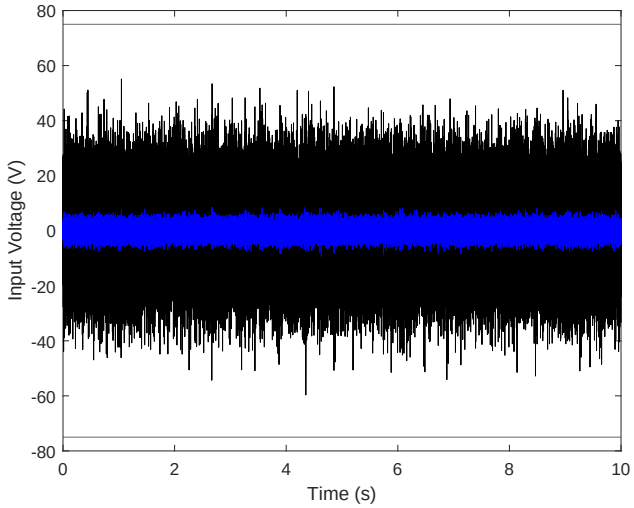

Figure 16: Voltage signal to the piezo actuators versus time for the (blue) initial model and (black) updated model.

As previously noted, the current limit proved to be the largest limiting factor to the shaker's performance. Figure 17 shows the electrical current signals from the initial and updated models, respectively. Again, the current signal for the updated model is about 7 times greater than that of the preliminary model. However, in contrast to our voltage signals, neither current signal falls within their specified limits. In the initial case, the current signal barely exceeds the proposed current limits. In the updated case, the current limits vastly exceed the limits.

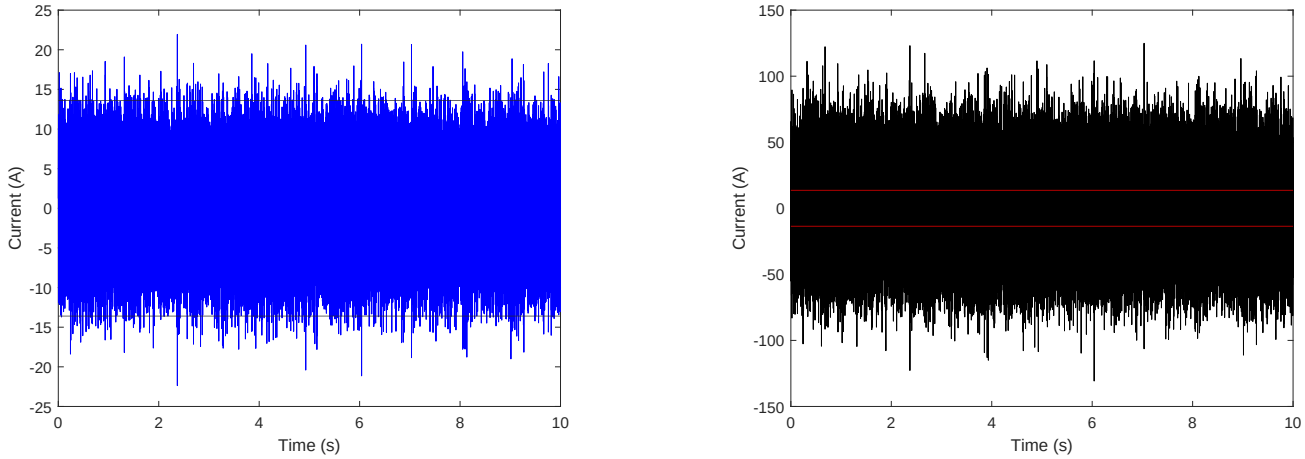

(a) Initial model

(b) Updated model

Figure 17: A time history of the current to the piezo actuators across our simulated time.

In order to understand the effect that the electrical current limits might have on the response of the system, the simulation was repeated, but this time clipping the current by setting it to its maximum or minimum value any time it exceeded the limits, as was described in Section 2.3. The clipped current signal was used to compute the voltage in the piezos, using Eq. (11) in the frequency domain. This was then used in Eq. (9) to recompute the forces in the piezo actuators. Those were applied to the system using Eq. (6). The resulting PSD of the environment at the DUT is shown in Fig. 18 and compared to that which would have been obtained if the amplifier had infinite current capability. The environment obtained using the initial model matches the original environment quite closely, because very little clipping occurred. In contrast, the current in the updated model is clipped dramatically. This changes the spectrum of the piezo force, reducing its amplitude from 1700-5000 Hz, while at the same time increasing its amplitude from 0 to 1700 Hz, which was initially zero. This spurious low-frequency content excites the 1200Hz resonance of the system, as seen in Fig. 13, because we did not reduce the force to the large shaker to compensate. At the same time, the response at higher frequencies reduces from 0.1 g^2/Hz to roughly 0.018 g^2/Hz because the spectrum of the piezo force was much lower at those frequencies due to the clipping. A shaker control system would update the forces in each of these actuators to compensate, but would be unable to reach the environment because any increase in the voltage to the piezos would cause increased clipping.

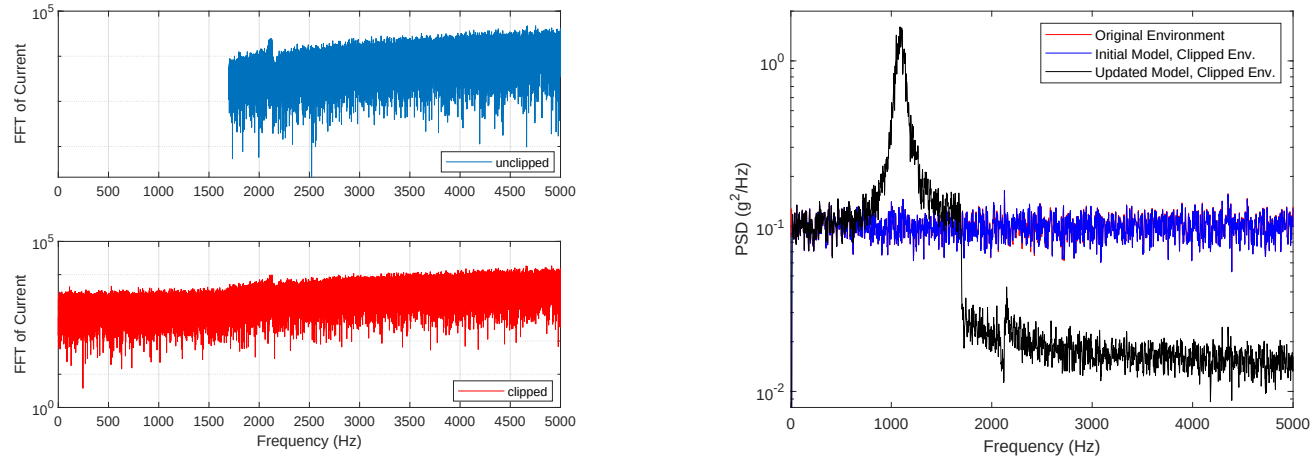

(a) Spectrum of the electrical current to the Piezo (blue) before and (red) after clipping.

(b) PSD of Environment at the DUT with the electrical current clipped.

Figure 18: Simulation of the effect of clipping the electrical current on the environment reconstructed at the control accelerometer.

3.3 Experimental Results

A variety of environmental tests were performed on the hardware that was manufactured as discussed in Sec. 2.1. The Data-Physics system was used to control to one of the accelerometers on the top plate, using the configuration discussed in Sec. 2.6.

The exact settings for the low and high pass filters used for the shaker and piezos are given in the caption for each result.

The goal was to recreate a target environment of 0.1 g^2/Hz, yet the system was not capable of reproducing an environment at that level. The maximum recreated environment had a mean power spectral density of 0.03 g^2/Hz, although this was a result of asking for 0.05 g^2/Hz from the controller. Figure 19 shows the auto-power spectra of the control accelerometer for this environment and also 0.01 g^2/Hz and 0.001 g^2/Hz environments. Somewhat similar to what was observed in the simulations with current clipping, the response for the 0.05 g^2/Hz environment shows over-excitation of the 1200 Hz resonance, and under-excitation of the high frequencies. In contrast, the controller was able to more accurately recreate the 0.01 g^2/Hz environment. Even then, both environments were not reproduced very accurately, with several frequencies exceeding the 6 dB tolerances that are shown with horizontal lines.

One notable feature of both experimental environments is the presence of strong anti-resonances at about 820 and 860 Hz. The system contains two rocking modes at 815.6 and 991.1 Hz, as seen in Figure 12. This suggests that the 820 and 860 Hz anti-resonances involve rocking motion of the system. Originally, the high-pass filter applied to the piezo actuators was set at 1400 Hz, forcing the shaker and piezos to create the low and high frequency portions of the environment, respectively. However, during testing, these anti-resonances resulted in excessive voltages being sent to the shaker, limiting the achievable acceleration environment. For this reason, the high-pass filter was set below 800 Hz, allowing the piezo actuators to assist the shaker in overcoming these anti-resonances. This anti-resonance is also associated with a significant peak in the stretching of the piezos, as can be seen in Figure 22, which is discussed later.

The responses in Figure 12 also show large spikes in acceleration at about 3800 Hz. These seem to come about because of the current clipping; these spikes were not visible in the data when controlling to an environment of 0.001 g^2/Hz; in that case our simulation model suggests that clipping would not occur. None of the measurements acquired in this work showed a mode at 3800 Hz.

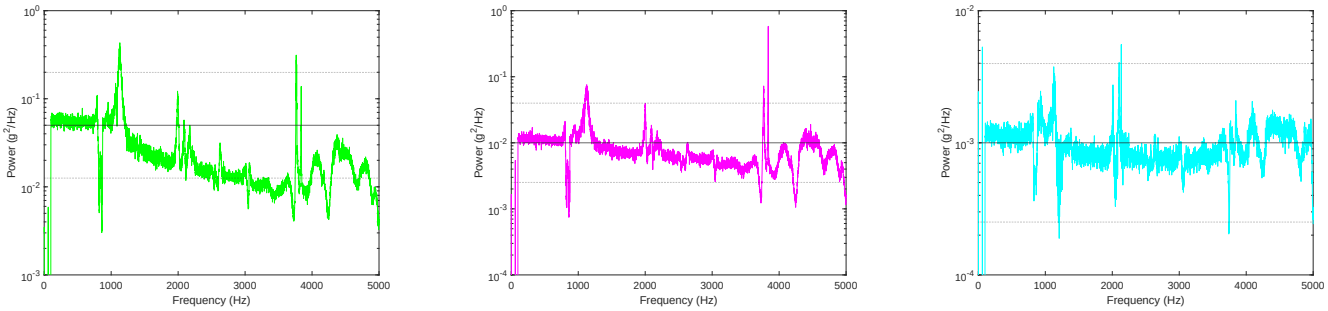

(a) Control environment of 0.05 g^2/Hz with high- and low-pass filters applied at f_{HP} =700 and f_{LP} =1800 Hz.

(b) Control environment of 0.01 g^2/Hz with high- and low-pass filters applied at f_{HP} =500 and f_{LP} =1800 Hz.

(c) Control environment of 0.001 g^2/Hz with high- and low-pass filters applied at f_{HP} =1400 and f_{LP} =1800 Hz.

Figure 19: PSD of the control accelerometer for the actual experiments for the target environment listed, with the high- and low-pass filters configured as described in Section 2.6. Controlled to the outside accelerometer as seen in 9c.

3.3.1 Comparison to model

Figure 20 compares these experimental environments to those predicted by our clipping model. Interestingly, at high frequencies, the measured spectrum at the control accelerometer for the highest amplitude (0.05 g^2/Hz) environment roughly matches the predicted output by the updated model, which included current clipping. Additionally, the experimental results include a large acceleration peak at about 1200 Hz, similar to the distortion caused in the model that included current clipping. Both these facts seem to indicate that our electrical current model reasonably tracks the true experimental behavior of the system.

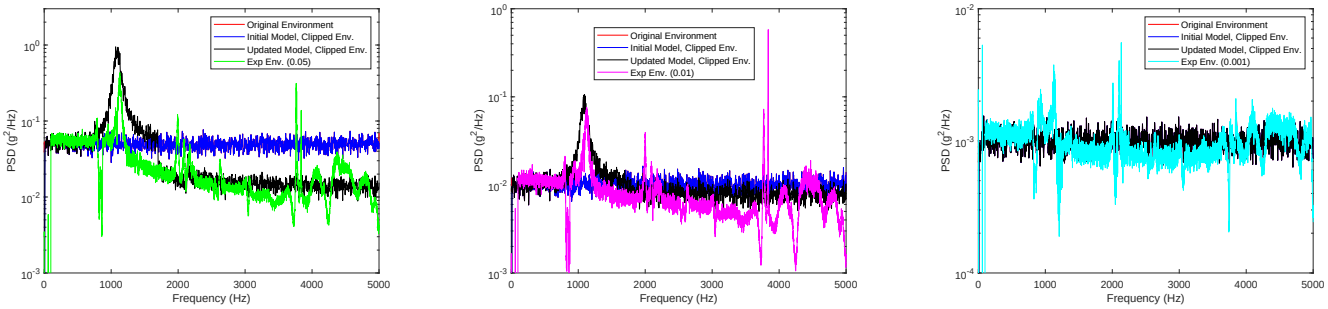

(a) 0.05 g^2/Hz (b) 0.01 g^2/Hz (c) 0.001 g^2/Hz

Figure 20: Comparison between ideal, experimental, and modeled acceleration environments at the control accelerometer.

The voltage sent to the piezos is compared to that predicted by the model in Fig. 21. The case considered is that of the 0.001 g^2/Hz target environment, where clipping should be minimal. Figure 21 shows that the updated model captures the overall magnitude of the piezo voltages reasonably well. The RMS voltages of the updated model and experiment are 1.33 and 1.15, respectively; the model slightly overestimates the piezo voltages. The model does not capture the variations in the voltage with frequency, which are quite significant in the experimental results. These presumably arise due to higher modes in the system that were not included in the model.

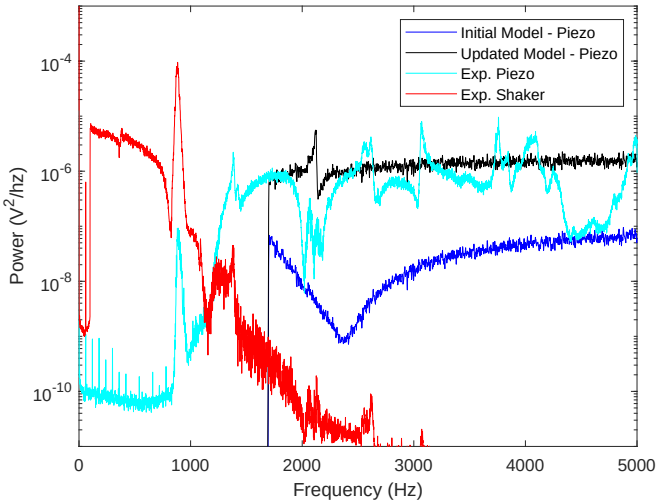

Figure 21: Comparison between auto power spectra of Piezo and Shaker voltage of the experiment and models for an environment of 0.001 g^2/Hz. Voltage powers are calculated from the control signals before amplification.

The measured strain is compared to the model predictions in Figure 22. Again, the case considered is that of the 0.001 g^2/Hz target environment, with high- and low-pass filters applied at f_{HP} =1400 and f_{LP} =1800 Hz respectively. The RMS values of the initial and updated models were 0.115 and 0.360 μm, respectively, and the figure shows that most of the displacement in the piezos occurred in the low frequency range. The experimentally measured strains show strong variations with frequency. The RMS of the measured strains from gauges 1 and 2 were 0.235 and 0.183 μm, respectively. They are dominated by a component at about 950 Hz and many other narrow-band components at various frequencies. The overall magnitude of the strain at low frequencies matches the initial model better than the updated model, but in any event it is clear that the model would need to include higher frequency dynamics to accurately capture the strain.

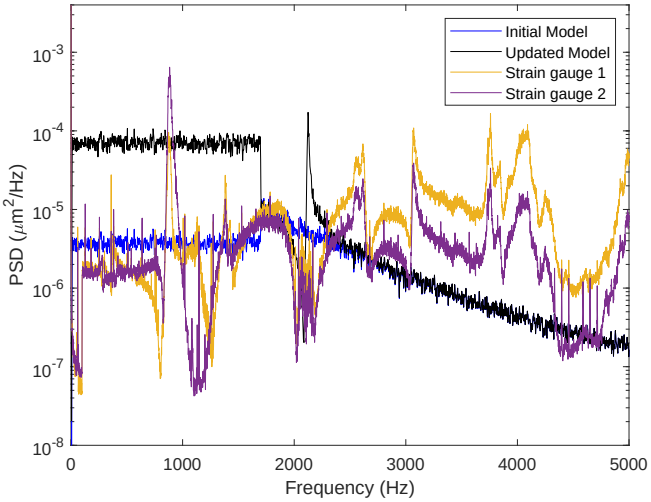

Figure 22: Comparison between auto power spectra of the piezo stretch of the experiment and models for an environment of 0.001 g^2/Hz. Strain gauges 1 and 2 refer to two strain gauges attached to two different piezo actuators during a single test.

3.3.2 Shaker Power Reduction

An additional experiment was performed to better understand the reduction in power required when incorporating piezo actuators. For this experiment, a given environment was created by only the shaker. Then, the same environment was recreated with the help of the piezo actuators. In this way, the required shaker voltage could be compared with and without the piezos.

The test was attempted with the original frequency range (0-5000Hz), but even for small environments the shaker encountered anti-resonances and could not adequately recreate high frequency environments by itself. Therefore, the upper frequency was reduced to 2800 Hz and to avoid any possibility of damage to the shaker, the environment level was decreased to (0.001 g^2/Hz) for this test.

As seen in Figure 23, the introduction of the piezo actuators significantly reduces the voltage sent to the shaker from roughly 10^{-6} to 10^{-10} V^2/Hz at high frequencies. At these frequencies, the piezos almost single-handedly recreate the environment requiring voltage levels that are similar to those required in the shaker-only test. Note that the voltages shown are those sent to the respective amplifiers. The amplifier for the electromagnetic shaker is a three-phase, 480 volt amplifier that measures $1.8 \times 0.8 \times 0.5$ m and weighs 500 kg. It can produce up to 80 amps of output current RMS and requires a large and noisy cooling system. In contrast, the piezo amplifiers each measure about $100 \times 150 \times 400$ mm (contained in a case the size of a desktop computer) and produce a total of 6.8 amps each. Hence, even though the voltage sent to these systems is similar, the total power required is dramatically different.

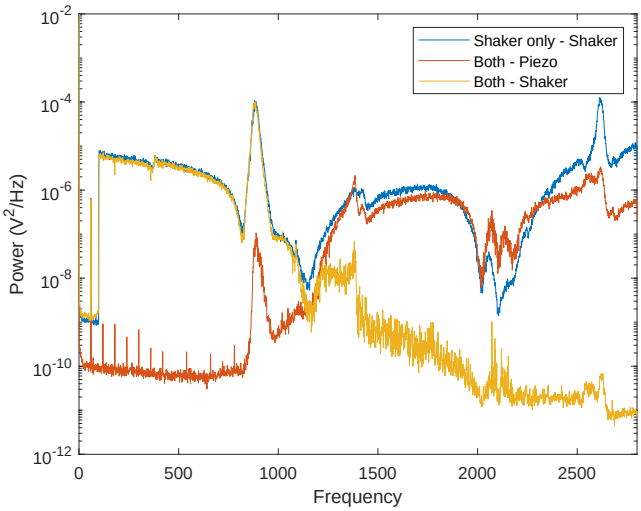

Figure 23: Comparison of shaker and piezo effort for an environment of 0.001 g^2/Hz from 50 to 2800 Hz for two cases. In the first, only the shaker is active. In the second, both shaker and piezo work together to create the environment. High- and low-pass filters applied at f_{HP} =1400 and f_{LP} =1800 Hz, as described in Section 2.6. The voltages shown are those sent to the respective amplifiers.

4 Conclusion

This work presented the design, modeling and testing of a system that integrates four piezoelectric actuators with a traditional, large electromagnetic shaker system. The goal of the system was to enable testing to higher frequencies, while avoiding damage to the electromagnetic shaker or piezo actuators. In its current form, the system failed to reproduce the 0.1 g^2/Hz environments that it was designed to reproduce, and it exhibited many spurious resonances and hence was generally not able to produce the PSD at the control accelerometer with reasonable fidelity. However, the effort so far has validated many aspects of modeling and provides several valuable insights into how such a system could be designed.

The most important finding was that the piezoelectric actuators require far more current than was expected in order to move a sizable DUT at high frequencies. The main limitation of the present design was linked to the electrical current limits of the amplifiers that were used to drive the piezoelectric actuators. If we had access to four of the present amplifiers, so that one could be used for each piezo, then our updated model predicts that we could have reproduced an environment up to $0.008 \frac{g^2}{Hz}$ with little to no clipping. That is for an upper frequency limit of 5 kHz. If the upper limit were reduced to 4 kHz, then the system with four amplifiers would be able to reach an environment of $0.016 \frac{g^2}{Hz}$. Alternatively, if unlimited current was available, our updated model predicts that we could have reproduced a 5 kHz environment up to $0.19 \frac{g^2}{Hz}$ or driven a payload of roughly 1.2 kg at the target environment of $0.10 \frac{g^2}{Hz}$ before other limitations posed an issue. According to our updated model, the next limitation to be reached is voltage, not strain. The present design could also be easily modified to allow up to eight piezo actuators (see the Appendix, Figure 25), increasing the capabilities further.

In designing the system, it was decided to maximize the frequency of the bubble mode of the top plate. In the final design, the natural frequency of the bubble mode was 3500 Hz with free boundary conditions; a similar mode appeared at 3000 Hz in the assembled system. However, the top plate that was designed was quite heavy and this exacerbated the problems with the piezo current. Furthermore, the assembled system still has a mode at only 1200 Hz where the top plate bounces on the piezo actuators. In retrospect, it may have been more effective to have designed the system to minimize the weight of the top plate, driving the bounce mode up and allowing the top plate bubble mode to decrease somewhat. The models developed here could be used to predict the behavior of such a system and develop a more optimal design. For example, according to the updated model, cutting the mass of the top plate in half would reduce the RMS current required by the piezos (i.e. see Fig. 17) from 28.6 A to 17.4 A, and the maximum current from 125 A to 72 A.

The test results showed several narrow ranges of frequencies in which the response exceeded or fell short of the desired environment. These frequencies are presumed to correspond to resonances and antiresonances of the system. The present configuration of the system does not seem to be sufficient to eliminate all of the antiresonances that occur below 5 kHz. Indeed, the modal test results in Sec. 3.1 show that the system has several resonances, and that the resonances all exhibited motions that coupled with axial motion of the system. Some experiments were performed in which pairs of piezo actuators were controlled separately, in hopes of allowing the system to overcome the antiresonances, but none of these was successful. For future

designs, we recommend using a higher fidelity finite element model to predict the resonances and antiresonances of the system, and then to see if the piezo actuators can be placed in such a way that they eliminate the antiresonances below 5 kHz.

Finally, some minor design improvements are suggested. For example, with the present design, a special low-profile socket wrench was needed to tighten the bolts to the piezo mounting brackets, because of the tight clearance between the piezo actuators. As shown in Fig. 25, the top plate and piezo mounting brackets could be modified to allow the central bolts to be tightened from above, greatly simplifying the assembly process.

5 Acknowledgements

The original shaker-piezo design configuration was developed by a BYU capstone team consisting of: McKaelin Edralin, Jonathan Paul, Nicholas Harris, Christian J. Johanson, Joel Gibb, and Corry Price. The authors are grateful for each of their contributions, which made this work possible.

References

[1] Washington J DeLima and Melanie N Ambrose. Experimental Characterization and Simulation of Vibration Environmental Test. In *Topics in Modal Analysis*, volume 10, pages 45–55. Springer, 2015.

[2] Vicente J. Romero, John V. Burkardt, Max D. Gunzburger, and Janet S. Peterson. Comparison of pure and "Latinized" centroidal Voronoi tessellation against various other statistical sampling methods. *Reliability Engineering and System Safety*, 91(10-11):1266–1280, 2006. Number: 10-11.

[3] A. Singh, M.S. Allen, M. Schmidt-Landin, and W.J. DeLima. Multi–Input Multi–Output Hybrid Active Vibration Control for High Frequency Random Vibration. *Experimental Techniques*, 46(1):67–79, February 2022.

[4] Physik Instrumente. Electrical operation of piezo actuators. `https://www.physikinstrumente.com/en/expertise/technology/piezo-technology/properties-piezo-actuators/electrical-operation`, 2025. Accessed: 2025-06-17.

[5] S. Sherrit, Christopher Jones, Jack Aldrich, Chad Blodget, Xiuliang Bao, Mircea Badescu, and Yoseph Bar-Cohen. Multilayer piezoelectric stack actuator characterization. *Proceedings of SPIE - The International Society for Optical Engineering*, 6929, 05 2008.

6 Appendix

6.1 Alternative Mounting Bracket Design

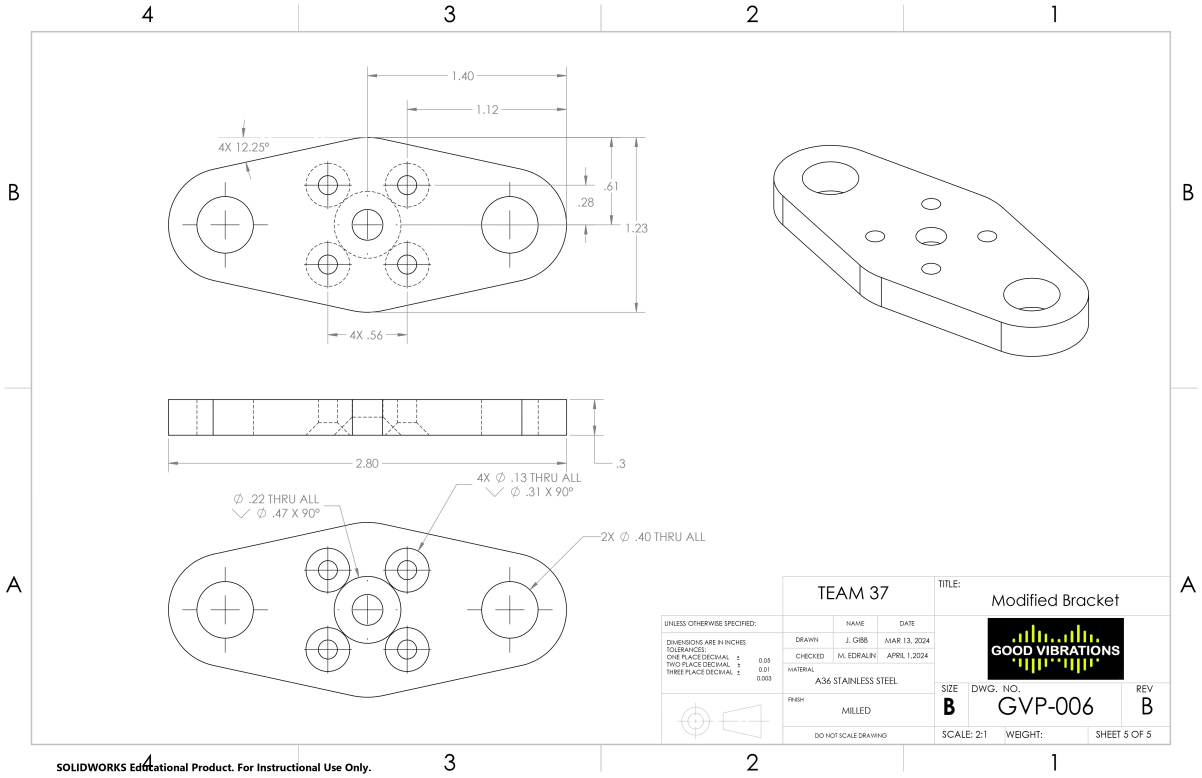

Figure 24: Modified mounting bracket that allows for four to eight piezo actuators.

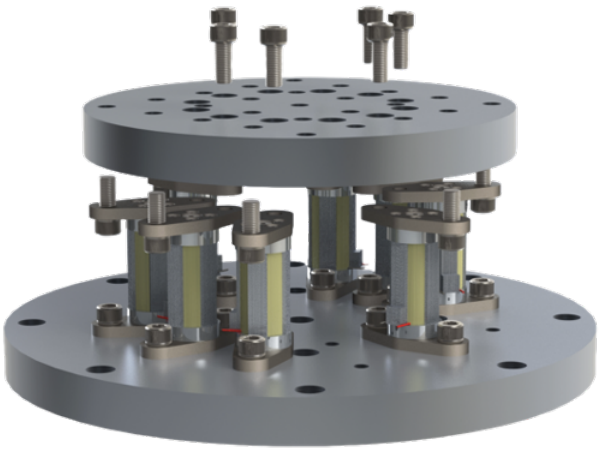

Figure 25: CAD rendering of an improved design with 8 piezo actuators and mounting screws accessible from above.

6.2 Assembly Instructions

The setup of the piezo assembly must be done meticulously to prevent damage and ensure proper functionality. The following are the steps and precautions used to set up a full piezo assembly test, with four piezo actuators.

1. Prepare all components: All parts must be properly prepared before assembly. For instance, the mounting brackets, top plate, and bottom plate need to be deburred, sanded down to a smooth finish, and cleaned. There should be no edges that would prevent the mounting bracket from sitting flush with its contact surfaces.

2. Check flat head screw clearances: The piezoelectric actuators contain a quartz crystal, which expands when a voltage is applied. The mounting screw locations on piezo actuators are through holes. This means that if the screws are tightened too much, it could crack the quartz and therefore break the piezo actuators. During assembly, put the screws in the mounting bracket and measure how much the screw extrudes. If it measures more than 6 mm, the mounting bracket should not be used.
3. Piezo and mounting bracket assembly: Mount a bracket to each end of the piezo actuator, using two brackets per piezo actuator.
4. Measure the piezo and bracket assembly: This is done to ensure the piezo actuator and mounting brackets are level and to determine the height of this assembly. It is best to measure two locations to ensure the piezo actuators are flush with the mounting brackets and level.
5. Base Plate: Mount it to the electrodynamic shaker
6. Bracket - Piezo assembly: Mount the piezo actuator bracket assemblies to the base plate. Tighten the brackets to the base plate with equal torque. Use shim stock as needed to keep the piezo actuators level.
7. Top Plate: Attach the top plate to the top of the mounting brackets
8. DUT: Attach the DUT to the top plate
9. Power and Software: power the piezo actuators and electrodynamic shaker. Also, run the software needed for tests.

This order of operations was sufficient to prevent any piezo actuators from being damaged during assembly.